Calibration Assessment and Boldness-Recalibration for Binary Events

Adeline P. Guthrie
Department of Statistics, Virginia Tech
and
Christopher T. Franck*
Department of Statistics, Virginia Tech

May 9, 2023

Abstract

Probability predictions are essential to inform decision making in medicine, economics, image classification, sports analytics, entertainment, and many other fields. Ideally, probability predictions are (i) well calibrated, (ii) accurate, and (iii) bold, i.e., far from the base rate of the event. Predictions that satisfy these three criteria are informative for decision making. However, there is a fundamental tension between calibration and boldness, since calibration metrics can be high when predictions are overly cautious, i.e., non-bold. The purpose of this work is to develop a hypothesis test and Bayesian model selection approach to assess calibration, and a strategy for boldness-recalibration that enables practitioners to responsibly embolden predictions subject to their required level of calibration. Specifically, we allow the user to pre-specify their desired posterior probability of calibration, then maximally embolden predictions subject to this constraint. We verify the performance of our procedures via simulation, then demonstrate the breadth of applicability by applying these methods to real world case studies in each of the fields mentioned above. We find that very slight relaxation of calibration probability (e.g., from 0.99 to 0.95) can often substantially embolden predictions (e.g., widening Hockey predictions' range from 25%-75% to 10%-90%).

Keywords: Calibration, Prediction, Bayesian Statistics, Model Selection

^{*}Corresponding author

1 Introduction

Probability predictions are made for everyday events, from the mundane, like the probability it will rain, to the life-altering, like the probability that a natural disaster hits a particular city. These predictions arise from both sophisticated statistical and machine learning techniques and/or simply from human judgement and expertise. Regardless, probability predictions are commonly used in important decision making processes in the fields of medicine, economics, image recognition via machine learning, sports analytics, entertainment and many others, so it is critical that we have methods that assess such predictions. The purpose of this paper is to develop methods for calibration assessment and boldness-recalibration that enable forecasters to achieve well calibrated, responsibly bold predictions for binary events.

We describe the assessment of probability predictions in terms of three aspects: calibration, accuracy, and boldness. The first aspect is calibration. Predicted probabilities are considered to be well calibrated when they are consistent with the relative frequency of events they aimed to predict. For example, if the home team wins 40% of games for which a Hockey forecaster predicted a 40% chance of a win, the forecaster is well calibrated. Probability calibration is well-studied within the fields of statistics, meteorology, psychology, machine learning, and others (Bross 1953, Murphy & Winkler 1977, Dawid 1982, DeGroot & Fienberg 1983, Gonzalez & Wu 1999, Guo et al. 2017). Naturally, calibration is considered a minimal desirable property of predicted probabilities (Dawid 1982). Without calibration, if a forecaster says the probability of a home team win is 70%, you cannot rely on that prediction to reflect the true probability of a win. However, well calibrated predictions are not necessarily accurate nor bold enough to be useful.

The second aspect to assess probability predictions is classification accuracy. Classification accuracy measures how well predictions distinguish between the events they aim to predict. Receiver-Operating Characteristic (ROC) curves and the corresponding area under the ROC curve (AUC) are frequently used to assess classification accuracy for probability predictions. These accuracy assessments do not measure calibration since any monotone transformation applied to forecaster probability predictions will produce the same ROC curve and AUC as the original predictions.

The third aspect to assess probability predictions is boldness. Forecasters exhibit greater boldness when their predictions are further from the sample proportion of events. For example, in National Hockey League (NHL) games in the 2020-21 season, the home team won 53% of games, thus the sample proportion is $\hat{p} = 0.53$. A Hockey forecaster who simply predicts the base rate of 0.53 for every NHL game is well calibrated, but lacks the boldness needed for actionable predictions. However, forecasters who produce bold predictions alone without calibration or good classification show they have misplaced confidence in their prediction ability.

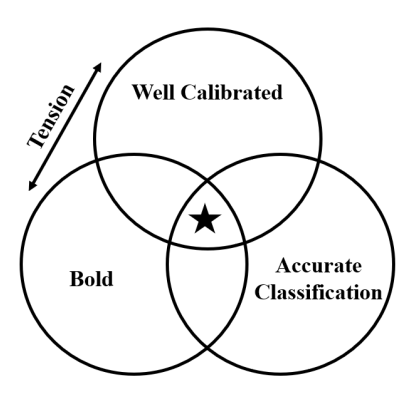


Figure 1: Venn Diagram highlighting the possible combinations of three aspects of probability predictions: calibration, boldness, and classification accuracy. We propose a boldness-recalibration approach that enables forecasters to maximize boldness while maintaining a high probability of calibration, subject to their classification accuracy.

This brings into focus the core tension between calibration and boldness, subject to classification accuracy. Notice the star in Figure 1 at the center of the three aspects. This intersection is where forecaster predictions are accurate, well calibrated, reasonably bold, and thus, actionable for decision making. The purpose of this paper is to show how good forecasters can position themselves at the center of the diagram.

Several methods exist for assessing calibration, but few consider boldness. Reliability diagrams plot the predicted forecaster probabilities versus the observed frequency within each bin (Murphy & Winkler 1977). The Brier Score can be decomposed such that one component directly measures calibration (Brier 1950, Murphy 1972, 1973). Another metric, called expected calibration error (ECE), reports the average calibration error across bins. However, the reliability diagram, Brier Score calibration component, and ECE lack natural

interpretability. Reliability diagrams require subjective assessment as they produce no numeric measure of calibration. The Brier Score and ECE are difficult to interpret on their own. We will show later that for our hockey forecaster data, the expert forecaster achieves a Brier Score of 0.23, while random noise predictions achieve a Brier Score of 0.27. There is no clear way for humans to pre-specify a meaningful difference in Brier Scores for an expert hockey forecaster and random noise.

Other methods go as far to correct mis-calibration, but still do not incorporate boldness in their adjustment. Dalton (2013) leverages the Cox linear-logistic model to test for calibration and proposes a relative calibration metric, but makes no mention of prediction boldness. Platt (2000) introduces Platt scaling which recalibrates Support Vector Machine (SVM) output via sigmoid curves. Guo et al. (2017) proposes recalibration via temperature scaling, a one-parameter extension of Platt scaling for Neural Network output. Zadrozny & Elkan (2001) propose a non-parametric approach called histogram binning where probabilities are bin-wise recalibrated to minimize squared loss. Zadrozny & Elkan (2002) extends this by fitting a piece-wise recalibration function on each bin interval. Naeini et al. (2015) extends this further to Bayesian Binning into Quantiles (BBQ) where multiple binning strategies are considered via Bayesian model averaging. However, none of these methods provide an interpretable measure of calibration, rather they rely on metrics like the Brier Score or ECE.

A few methods both recalibrate and embolden predictions in highly specific circumstances. Lichtendahl et al. (2022) focuses on aggregates of forecaster predictions and their spread but they specifically focus on a forecast aggregation approach that is not applicable to individual forecasters. We focus on appropriately emboldening predictions from a single forecaster subject to their calibration and classification accuracy. The five case studies we present are not aggregate forecasts, and thus the approach of Lichtendahl et al. (2022) is not applicable here. Turner et al. (2014), Baron et al. (2014), and Atanasov et al. (2017) also focus on aggregates, using the linear log odds (LLO) recalibration function to adjust aggregate boldness. Roitberg et al. (2022) employs a network based temperature scaling approach to recalibrate and correct overly bold softmax pseudo-probabilities. However, Turner et al. (2014), Baron et al. (2014), Atanasov et al. (2017) and Roitberg et al. (2022)

all rely on the Brier Score and/or ECE to assess calibration. Han & Budescu (2022) focus on LLO applied to forecasts of continuous, rather than binary, events. Gonzalez & Wu (1999) use LLO to recalibrate single forecaster predictions but focus solely on the psychological implications of probability perception for binary events. None of these methods provide a calibration testing approach nor direct control or clear interpretation of the calibration-boldness tradeoff.

To the best of our knowledge, no methodology yet exists that (a) uses a human-interpretable metric to quantify the boldness-calibration tradeoff, (b) is forecaster and method agnostic, meaning it operates only on probability predictions and event data, and (c) does not rely on binning. To address this gap in the literature, our goals are as follows. First, we want to test the plausibility of calibration in an interpretable manner. Second, we want to maximize boldness given a set level of calibration and provide a clear interpretation of the calibration-boldness trade-off. To achieve our first goal, we describe a Bayesian approach to obtain the posterior model probability that a forecaster's predictions are calibrated. To achieve our second goal, we propose boldness-recalibration. Boldness-recalibration allows users to set the desired level of calibration in terms of the posterior calibration probability and then maximizes boldness by maximizing spread in predictions subject to calibration level. By using these readily interpretable measures of calibration and boldness, we provide an intuitive interpretation of the calibration-boldness trade-off.

The rest of this paper is organized as follows. Section 2 introduces our methodology and pertinent real-world and simulation data examples. In Section 3, we provide the results of our simulated and real-world examples. Section 4 provides a discussion and concluding comments.

2 Methods

The following approaches are model agnostic, meaning they can be applied to any probability forecasts of binary events produced by forecasters from many domains. By forecaster, we mean any entity that produces probability predictions, regardless if they are machine learning output and/or a product of human judgement and expertise.

2.1 Linear Log Odds (LLO) Recalibration Function

To assess calibration, we use the linear log odds (LLO) recalibration function. Let $c(\mathbf{x}; \delta, \gamma)$ be the LLO function

$$c(\mathbf{x}; \delta, \gamma) = \frac{\delta \mathbf{x}^{\gamma}}{\delta \mathbf{x}^{\gamma} + (1 - \mathbf{x})^{\gamma}},\tag{1}$$

where \mathbf{x} is a set of probability predictions from a single forecaster, $\delta > 0$ and $\gamma \in \mathbb{R}$. We call the outputted probabilities, $c(\mathbf{x}; \delta, \gamma)$, the LLO-adjusted set of probabilities. The LLO-adjusted set is based on shifting and scaling the original forecaster probabilities \mathbf{x} on the log odds scale using δ and γ . Thus, on the log odds scale, the LLO-adjusted set is linear with respect to \mathbf{x} according to intercept $log(\delta)$ and slope γ , and can be re-written as

$$log\left(\frac{c(\mathbf{x};\delta,\gamma)}{1-c(\mathbf{x};\delta,\gamma)}\right) = \gamma log\left(\frac{\mathbf{x}}{1-\mathbf{x}}\right) + log(\delta), \tag{2}$$

Suitable choices of δ and γ can calibrate poorly calibrated probabilities. When both $\delta = 1$ and $\gamma = 1$, the LLO function imposes no shifting nor scaling, returning the original set \mathbf{x} (Gonzalez & Wu 1999). Thus, null values of $\delta_0 = \gamma_0 = 1$ corresponds to the hypothesis that \mathbf{x} is well calibrated.

2.2 Likelihood Function

We adopt a Bernoulli likelihood where the events are presumed independent and the probability of each event is governed by LLO-adjusted probabilities. Let \mathbf{y} be a vector of n outcomes corresponding to the n predictions in \mathbf{x} . Then, we have

$$\pi(\mathbf{x}, \mathbf{y}|\delta, \gamma) = \prod_{i=1}^{n} c(x_i; \delta, \gamma)^{y_i} \left[1 - c(x_i; \delta, \gamma)\right]^{1-y_i}.$$
 (3)

This likelihood enables calibration maximization via maximum likelihood estimates (MLEs) for δ and γ . The $\hat{\delta}_{MLE}$ and $\hat{\gamma}_{MLE}$ values produce optimally calibrated probabilities, $c(\mathbf{x}; \hat{\delta}_{MLE}, \hat{\gamma}_{MLE})$. Shifting via $\hat{\delta}_{MLE}$ on the log odds scale adjusts the average prediction to match the sample proportion. Scaling by $\hat{\gamma}_{MLE}$ on the log odds spreads out or contracts predictions based on accuracy. This may be a desirable approach when probability calibration is the sole priority.

2.3 Bayesian Assessment of Calibration

Using the likelihood function in the previous section, we take a Bayesian model selection-based approach to calibration assessment. We compare a well calibrated model, M_c (where $\delta = \gamma = 1$), to an uncalibrated model, M_{nc} (where $\delta > 0, \gamma \in \mathbb{R}$). The posterior model probability of M_c given the observed outcomes \mathbf{y} serves as our measure of calibration for the testing framework and can be expressed as

$$P(M_c|\mathbf{y}) = \frac{P(\mathbf{y}|M_c)P(M_c)}{P(\mathbf{y}|M_c)P(M_c) + P(\mathbf{y}|M_{nc})P(M_{nc})}.$$
(4)

Here, $P(\mathbf{y}|M_i)$ is the integrated likelihood of the observed outcomes \mathbf{y} given M_i and $P(M_i)$ is the prior probability of model $i, i \in \{c, nc\}$. A common approach when prior information about calibration is unavailable is to assign a uniform prior to the model space such that $P(M_c) = P(M_{nc}) = \frac{1}{2}$. The expression in (4) can be re-written as

$$P(M_c|\mathbf{y}) = \frac{1}{1 + BF_{21}}. (5)$$

where BF_{21} is the Bayes Factor for our two competing models and is defined as

$$BF_{21} = \frac{P(\mathbf{y}|M_{nc})}{P(\mathbf{v}|M_c)}. (6)$$

Using the likelihood in (3), the integrated likelihoods, $P(\mathbf{y}|M_i)$, are not analytically tractable. While a fully Bayesian approach could be implemented, we advocate for a useful approximation. We employ the Bayesian Information Criteria (BIC) approximation of BF_{21} such that

$$BF_{21} \approx exp\left\{-\frac{1}{2}(BIC_2 - BIC_1)\right\} \tag{7}$$

to form the posterior model probability in (5) (Kass & Raftery 1995). Here, the BIC under the well calibrated model M_c is defined as

$$BIC_1 = -2 \times log(\pi(\delta = 1, \gamma = 1 | \mathbf{x}, \mathbf{y})). \tag{8}$$

The penalty term for number of estimated parameters is omitted in (8) as both parameters are fixed at 1 under M_c . The BIC under poorly calibrated model M_{nc} is defined as

$$BIC_2 = 2 \times log(n) - 2 \times log(\pi(\hat{\delta}_{MLE}, \hat{\gamma}_{MLE} | \mathbf{x}, \mathbf{y})). \tag{9}$$

With this approximation for BF_{21} , we form $P(M_c|\mathbf{y})$, which can be interpreted as the probability the set of forecasts \mathbf{x} is well calibrated given the observed data \mathbf{y} . The interpretability of the posterior model probability, $P(M_c|\mathbf{y})$, is the key feature of this Bayesian test for calibration. By quantifying the calibration of probability forecasts with a readily interpretable metric, we enable easier comparison of forecasters in terms of calibration and more informed decision making.

2.4 Boldness-Recalibration

The previous Bayesian model selection approach assesses calibration alone with no regard for boldness. The goal of boldness-recalibration is to maximize the spread, or boldness of predictions subject to a user-specified constraint on the calibration probability, $P(M_c|\mathbf{y})$. To accomplish this we let the user set the calibration level, t, that $P(M_c|\mathbf{y})$ must achieve. For example, if we want to ensure our recalibrated probabilities had a posterior probability of at least 95%, we would set t = 0.95. Then boldness is maximized subject to $P(M_c|\mathbf{y}) = 0.95$.

To visualize the process of boldness-recalibration, consider the two schemas in Figure 2. The panel on the left depicts predictions that vary in boldness. The "less bold" predictions are closer to the base rate \hat{p} . The "more bold" predictions arise by moving the original predictions away from the base rate.

The panel on the right of Figure 2 shows a boldness-recalibration contour plot. This plot is used throughout the paper to show $P(M_c|\mathbf{y})$ across a grid of LLO-adjustment parameters δ and γ . Rather than focus solely on where $P(M_c|\mathbf{y})$ is high (i.e. high calibration), we can draw a contour at $P(M_c|\mathbf{y}) = t$ to focus on our user specified level of calibration. Then, along that contour we identify the δ and γ that maximize spread in the LLO-adjusted probabilities via a grid-search based approach. The δ and γ values corresponding to the star indicate precisely how to use Eq.(1) to embolden predictions subject to t. In Figure 2, we identify these parameters with the star along the red contour at t = 0.95. We call the LLO-adjusted probabilities under these parameters the 95% boldness-calibration set. Further details of the approach can be found in the online supplement.

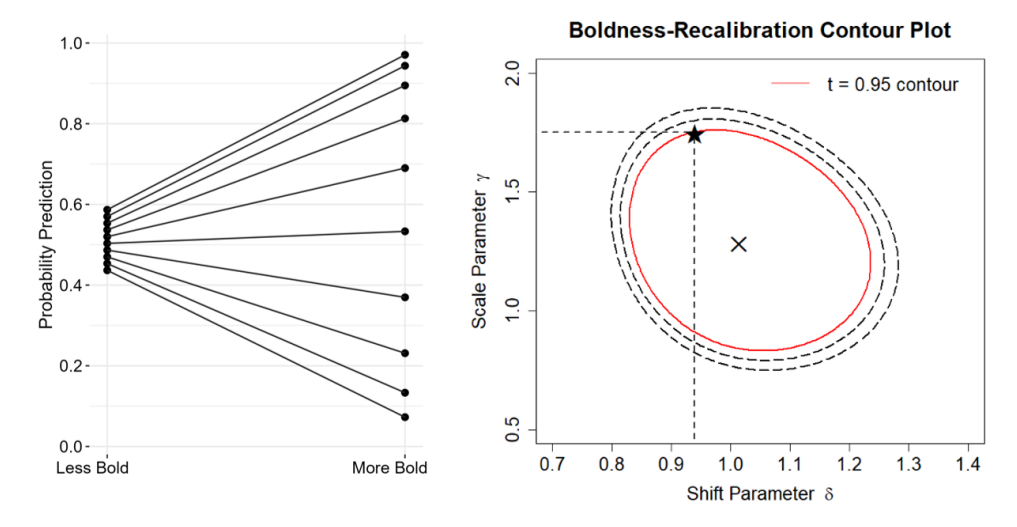


Figure 2: Schemas to visualize boldness-recalibration. The left panel shows boldness as a function of spread in predictions. Each line corresponds to a prediction. The right panel shows a boldness-recalibration contour plot where the x-axis is shift parameter δ , y-axis is scale parameter γ , and z-axis is $P(M_c|\mathbf{y})$ achieved by δ and γ . Contours correspond to $P(M_c|\mathbf{y}) = 0.95$ (solid red), 0.9 and 0.8 (dashed black). The \times corresponds to $(\hat{\delta}_{MLE}, \hat{\gamma}_{MLE})$ such that the resulting probabilities under LLO-adjustment have maximal probability of calibration. The star on the 0.95 contour corresponds to $(\hat{\delta}_{0.95}, \hat{\gamma}_{0.95})$ such that the resulting probabilities have maximal spread subject to 95% calibration. These LLO-adjusted probabilities are called the 95% boldness-recalibration set.

2.5 Likelihood Ratio Test for Calibration

Perhaps surprisingly, it does not appear as if a Likelihood Ratio Test (LRT) based on (3) has been previously proposed in the literature. We devise a frequentist approach to this problem by setting up a likelihood ratio test for the following hypotheses:

$$H_0: \delta = 1, \gamma = 1$$
 (Probabilities are well calibrated)
 $H_1: \delta \neq 1$ and/or $\gamma \neq 1$ (Probabilities are poorly calibrated)

Thus, the likelihood ratio test statistic for H_0 is

$$\lambda_{LR} = -2log \left[\frac{\pi(\delta = 1, \gamma = 1 | \mathbf{x}, \mathbf{y})}{\pi(\delta = \hat{\delta}_{MLE}, \gamma = \hat{\gamma}_{MLE} | \mathbf{x}, \mathbf{y})} \right], \tag{10}$$

where $\lambda_{LR} \stackrel{H_0}{\sim} \chi_2^2$ asymptotically under the null hypothesis H_0 . The above test statistic can be used to test the calibration of a vector of predicted probabilities, \mathbf{x} , and the vector of corresponding outcomes, \mathbf{y} .

2.6 Other Methods to Assess Calibration

We report the Brier Score and Expected Calibration Error for the examples in this paper.

2.6.1 Brier Score Calibration Component

For binary events, the Brier Score takes on the form

$$BS = \frac{1}{n} \sum_{i=1}^{n} (x_i - y_i)^2 \tag{11}$$

where x_i is the predicted probability for event i and y_i is the binary outcome (0 if a non-event, 1 if event). The Brier Score in (11) can take on any value from 0 to 1, where lower values are better.

The Brier Score can be decomposed as follows:

$$BS = \frac{1}{n} \sum_{k=1}^{K} (\mathbf{x}_k - \bar{\mathbf{y}}_k)^2 + \frac{1}{n} \sum_{k=1}^{K} n_k \bar{\mathbf{y}}_k (1 - \bar{\mathbf{y}}_k)$$
 (12)

where \mathbf{x}_k is the set of predicted probabilities within bin k and $\bar{\mathbf{y}}_k$ is the relative frequency of events corresponding to the observations in bin k (Murphy 1972). The first addend on the right hand side of (12) is a measure of calibration, which we will abbreviate as BSC, and is the measure we will compare to $P(M_c|y)$.

2.6.2 Expected Calibration Error (ECE)

We will also compare $P(M_c|\mathbf{y})$ with expected calibration error (ECE). For binary events, ECE takes on the form

$$ECE = \sum_{b=1}^{B} \frac{n_b}{n} |\bar{y}_b - \bar{x}_b|$$
 (13)

where B is the number of bins, n_b is the number of predictions partitioned into bin b, \hat{y}_b is the proportion of observed events in bin b, and \hat{x}_b is the average probability prediction in bin b. ECE can take on any value from 0 to 1, where lower values are better.

2.7 Data

2.7.1 Simulation Study

Table 1 shows the four forecaster types in our simulation study. The data generation process for our simulation follows:

1. Generate n true event outcomes via random independent Bernoulli draws, where the probability of success at each draw takes on a random uniform draw from 0 to 1.

$$p_i \sim \text{Uniform}(0,1), y_i \sim \text{Bernoulli}(p_i), i = 1, ..., n$$

The p_i s make up the well calibrated forecaster predictions by construction, as they directly correspond to the true probability of each event outcome.

2. To manipulate classification accuracy, add varying amounts of random noise, v_i , to each p_i on the log odds scale, which is equivalent to

$$p_{i,\sigma} = \frac{e^{v_i} p_i}{(1 - p_i) + e^{v_i} p_i}$$

where $p_{i,\sigma}$ is the set of noisy probabilities and $v_i \sim N(0, \sigma^2)$, $\sigma \in \{0, 0.1, 0.5, 1, 2\}$.

3. To manipulate boldness and create the four forecaster types, LLO-adjust $p_{i,\sigma}$ under varying δ and γ values, summarized in Table 1. Since the LLO function is monotone, forecasters LLO-adjusted from $p_{i,\sigma}$ maintain the same classification accuracy as $p_{i,\sigma}$.

Forecaster Type	δ	γ	Description
Well Calibrated	1	1	Ideal Forecaster
Hedger	1	0.25	Not Bold
Boaster	1	2	Too Bold
Biased	2	1	Too Optimistic for Event

Table 1: Values of δ and γ under which each forecaster type is simulated via the LLO-function and description of forecaster type.

The first forecaster type, called Well Calibrated, represents forecasters whose predictions correspond to the true event rate. Notice in Table 1 that these predictions are LLO-adjusted

under $\delta = \gamma = 1$, so the Well Calibrated Probabilities are equivalent to the perfectly calibrated probabilities with added noise, i.e. $p_{i,\sigma}^{wc} = p_{i,\sigma}$. Thus under $\sigma = 0$, $p_{i,0}^{wc} = p_i$, the perfectly calibrated probabilities.

Our second forecaster type is called Hedger. The Hedger compresses probabilities around the base rate, 0.5 in this case. We call their predictions "hedged" as they reflect forecasters who are lacking boldness even though their accuracy could be high. In contrast, our third forecaster type, Boaster, represents a forecaster who exhibits excessive boldness. The majority of their predictions are far from the base rate and very close to the extremes of 0 and 1. The fourth forecaster type is Biased. These forecasters systematically make predictions that are higher or lower than the event rate.

To explore the effect of sample size on our methodology, we generated data sets of size n = 30, 100, 800, 2,000, and 5,000. In total, we present results from 100 Monte Carlo (MC) replicates for each value of n. Throughout the study, one MC replicate consists of a set of n outcomes, and a corresponding set of n predicted probabilities for each of the four forecasters types under each of the five noise settings (20 total predicted probabilities sets for each replicate).

2.7.2 Hockey Home Team Win Predictions

To demonstrate the capabilities of boldness-recalibration, we assembled data from FiveThirtyEight that pertain to the 2020-21 National Hockey League (NHL) Season. FiveThirtyEight produced predicted probabilities for all 868 regular season games that season. These predictions were furnished prospectively pre-game, with no in- or post-game updating. FiveThirtyEight probabilities are potentially hedged towards the base rate of 0.53 with an inter-quartile range is 0.12 (0.47, 0.59), their full range being (0.26, 0.77).

In addition to this real-world forecaster, we generated a set of 868 random probability predictions to represent hockey forecaster who is completely uniformed about the NHL games they aimed to predict. We call this forecaster our "Random Noise" forecaster. To mimic this behavior and better enable comparability, our Random Noise forecaster is generated by taking random uniform draws from 0.26 to 0.77, the observed range in the FiveThirtyEight data.

2.7.3 Boldness-recalibration for case studies

We apply our calibration assessment, boldness-recalibration approach, ECE, and the Brier score to case studies in foreclosure monitoring (Keefe et al. 2017), biostatistics (Levine et al. 2013), Academy Award prediction (Franck & Wilson 2021), and image classification (Krizhevsky et al. 2009). More details about these projects and data can be found in the online supplement.

3 Results

3.1 Simulation Study

Figures 3, 4, and 5 summarize $P(M_c|\mathbf{y})$, the LRT p-value, and BSC for the 100 MC runs. On each figure, the boxplots are grouped by simulated forecaster type shown on the x-axis. The y-axis shows the value of the metric of interest. Sample size increases with vertical panels from top to bottom. Within each group of boxplots, added noise σ increases from left to right. Thus, for the Well Calibrated group, only the first boxplot with no added noise ($\sigma = 0$) is perfectly calibrated and both calibration and accuracy decrease as noise increases.

The posterior model probability of calibration, $P(M_c|\mathbf{y})$, is summarized in Figure 3. We expect $P(M_c|\mathbf{y})$ to be high for well calibrated forecasters and low for poorly calibrated forecasters. As sample size increase, $P(M_c|\mathbf{y})$ decreases for all settings except the Well Calibrated forecasters with little to no added noise. This indicates our Bayesian approach performs sensibly in that the ability to correctly detect miscalibration increases with sample size. Additionally, as more noise is added to the Well Calibrated forecaster, their probability of calibration decreases as expected. Notice that under low sample sizes, Hedgers with large added noise appear well calibrated. This is not surprising as we have already established that hedging predictions with poor classification accuracy is a favorable strategy to achieve calibration.

Figure 4 shows that as sample size increases, the LRT p-value for calibration also decreases in all settings except for the Well Calibrated forecasters with little or no noise, where the null hypothesis is true by construction (and thus p-values are uniform). This

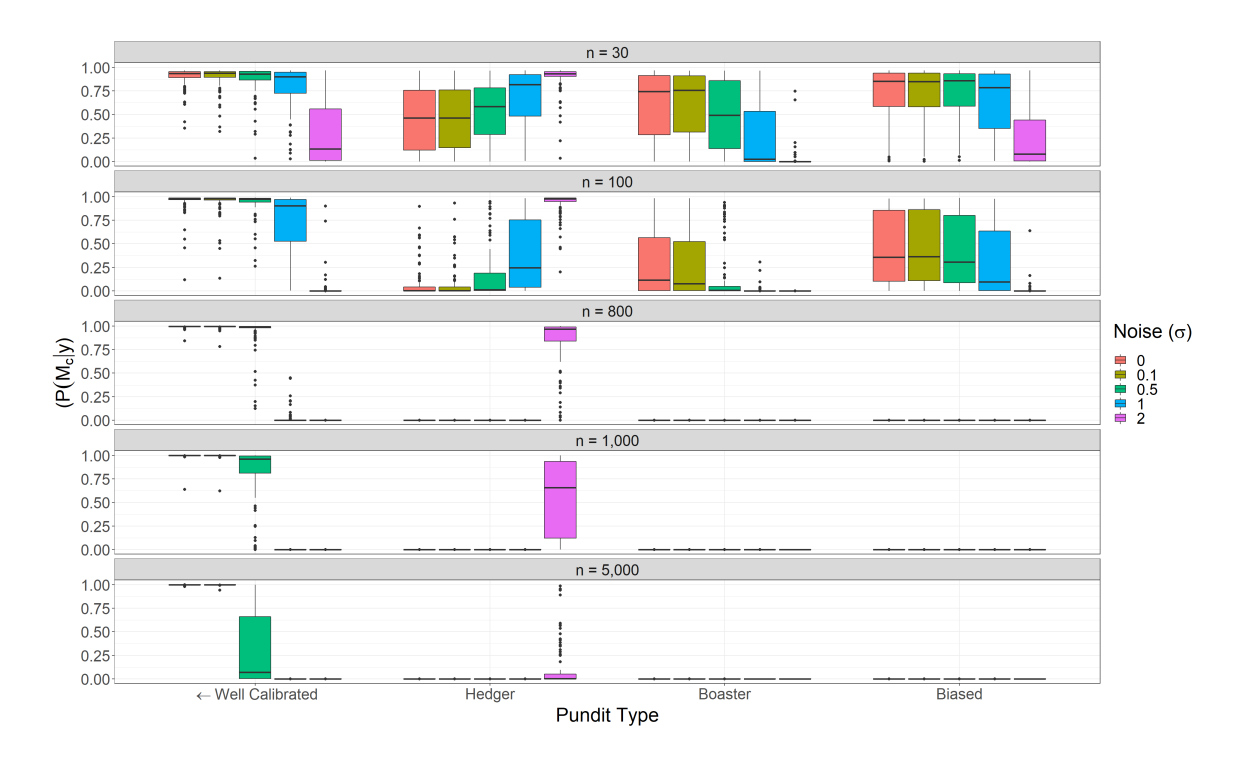


Figure 3: Boxplots summarizing the posterior model probability of calibration, $P(M_c|\mathbf{y})$, on the y-axis for 100 MC runs on simulated forecasters. Boxplots are grouped by forecaster type on the x-axis. Within groups, added noise increases from left to right. Only the leftmost boxplot in the Well Calibrated group is perfectly calibrated, and \leftarrow indicates calibration increases as noise decreases. As sample size increases with vertical panels, $P(M_c|\mathbf{y})$ decreases for all forecasters except Well Calibrated with little to no added noise.

reflects increasing power to detect miscalibration with increasing sample size. Again, notice that Hedgers with large added noise appear well calibrated, but as power increases, our LRT more easily detects the miscalibration.

Figure 5 shows that as sample size increases the BSC decreases for all settings, not just those that are well calibrated. Recall smaller BSC reflects greater calibration. At large sample sizes, the Hedger with large added noise score is nearly indistinguishable from the perfectly calibrated forecaster on the far left. While BSC for the Boasters and Biased forecasters are higher than the well calibrated, the difference in marginal. Overall, the distinction between forecasters is much smaller under this metric. Unlike posterior probability of calibration, it is difficult to interpret an individual forecaster's Brier Score in isolation.

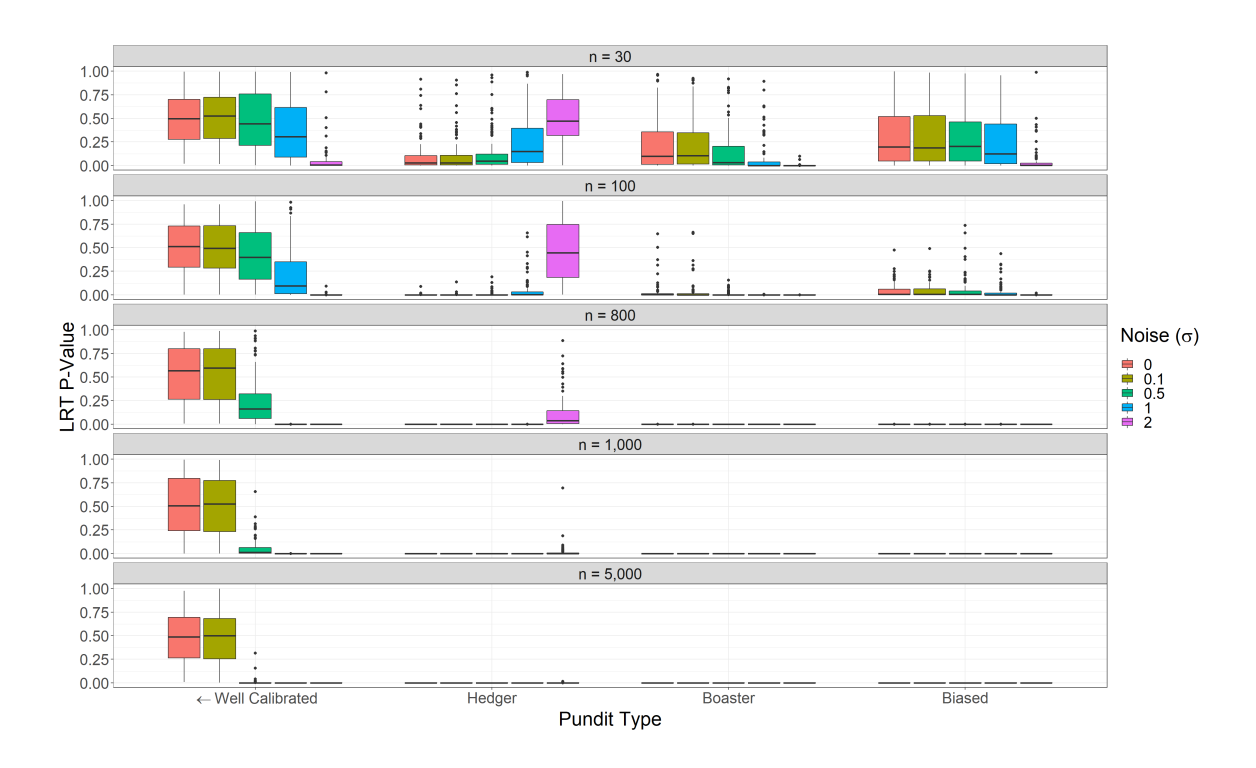


Figure 4: Boxplots summarizing the LRT p-value on the y-axis for 100 MC runs on simulated forecasters. Boxplots are grouped by forecaster type on the x-axis. Within groups, added noise increases from left to right. Only the leftmost boxplot in the Well Calibrated group is perfectly calibrated, and ← indicates calibration increases as noise decreases. As sample size increases with vertical panels, the p-value decreases for all forecasters except Well Calibrated with little to no added noise. Instead we see uniformly distributed p-values for these Well Calibrated forecasters as expected.

3.2 Hockey Home Team Win Predictions Case Study

3.2.1 Assessing Calibration

Table 2 summarizes the $P(M_c|\mathbf{y})$, LRT p-value, Brier Score, Brier Score Calibration, ECE, and AUC for FiveThirtyEight and our Random Noise forecaster. Both of our proposed approaches to calibration assessment successfully identify FiveThirtyEight as well calibrated and Random Noise as poorly calibrated. The probability of calibration given the event outcomes for FiveThirtyEight is very high at 0.9904, whereas the probability for Random Noise rounds down to 0.0000. This shows there is a definitive difference in calibration between the two forecasters, as we would expect. The LRT p-values agree with this assess-

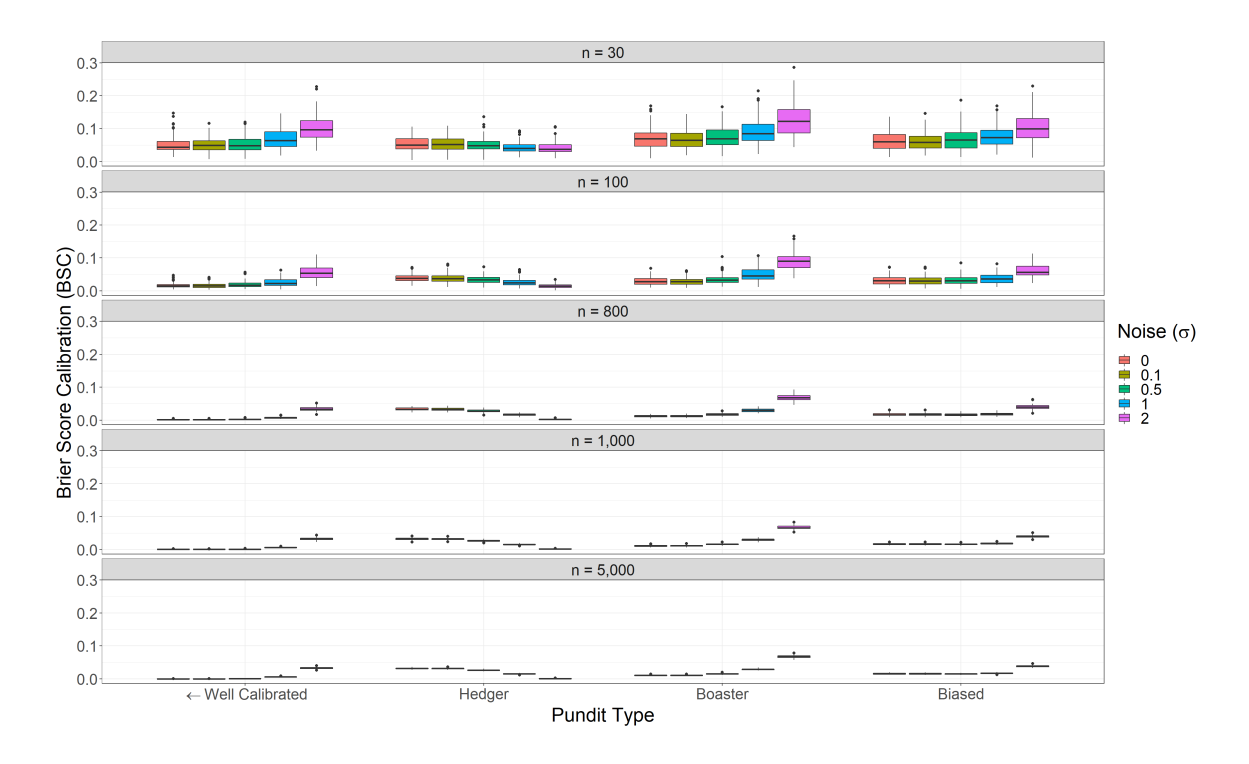


Figure 5: Boxplots summarizing the BSC on the y-axis for 100 MC runs on simulated forecasters. Boxplots are grouped by forecaster type on the x-axis. Within groups, added noise increases from left to right. Only the leftmost boxplot in the Well Calibrated group is perfectly calibrated, and \leftarrow indicates calibration increases as noise decreases.

ment, as the p-value is high for FiveThirtyEight, at 0.1184, and very small for Random Noise, close to 0.

Forecaster	$P(M_c y)$	P-Value	Brier Score	BSC	ECE	AUC
FiveThirtyEight	0.9904	0.1184	0.2346	0.0022	0.0520	0.6475
Random Noise	0.0000	< 0.001	0.2675	0.0189	0.1243	0.5119

Table 2: Values of the posterior model probability of calibration $P(M_c|\mathbf{y})$, LRT p-value, overall Brier Score, Brier Score calibration component (BSC), expected calibration error (ECE), and area under the ROC curve (AUC) achieved by the original probability predictions of FiveThirtyEight and Random Noise.

In terms of the Brier Score, FiveThirtyEight and Random Noise achieve scores of 0.2346 and 0.2675 respectively. While the Brier Score for Random Noise is higher, the difference

is marginal at just 0.0329. For a more direct measure of calibration, the Brier Score Calibration component achieved by FiveThirtyEight and Random Noise are 0.0022 and 0.0189 respectively. Again, this results in a difference of 0.0167. It is hard to say how this practically translates to how much "better" FiveThirtyEight is compared to Random Noise and what a 'good" Brier Score is for this application. Yet FiveThirtyEight are experts and Random Noise is nonsense. ECE suffers from a similar problem, with FiveThirtyEight scoring at 0.0520 and Random Noise at 0.1243. This produces the most meaningful difference of the three metrics at 0.0723, but still lacks natural interpretability. The difference in $P(M_c|\mathbf{y})$ between the two forecasters is more clear and interpretable.

In terms of classification accuracy, FiveThirtyEight produces an AUC of 0.64. This implies their predictions are better than chance and provide some information in classifying a home team win. Our Random Noise forecaster produces an AUC of 0.51, which is very close to the underlying 0.5 we would expect as this forecaster makes predictions completely via random chance.

3.2.2 Boldness-Recalibration

We applied boldness-recalibration to the two Hockey forecasters at three specified levels of calibration: t = 0.95, 0.9, and 0.8. Figure 6 shows the boldness-recalibration plots for FiveThirtyEight (Left) and Random Noise (Right). Regions in red show where $P(M_c|\mathbf{y})$ is high for the LLO-adjusted \mathbf{x} via the corresponding δ (x-axis) and γ (y-axis) values. Regions in blue show where $P(M_c|\mathbf{y})$ is low. As expected, $\hat{\delta}_{MLE}$ and $\hat{\gamma}_{MLE}$, marked by the white \times in Figure 6, lie at the point where the probability of calibration is maximized. The values for $\hat{\delta}_t$ and $\hat{\gamma}_t$ are marked by white points along the contour for each t. Recall these represent the set of LLO-adjustment parameters for which maximal boldness is achieved with a probability of calibration of at least t. These parameter values, along with the achieved $P(M_c|\mathbf{y})$, are summarized in Table 3. The sliver shaped region at $\gamma = 0$ zero is not useful for boldness-recalibration and can be ignored because it maps all predictions to the base rate.

After deploying boldness-recalibration on the two sets of predictions, we see a substantial increase in boldness for FiveThirtyEight. Figure 7 shows how the predictions for

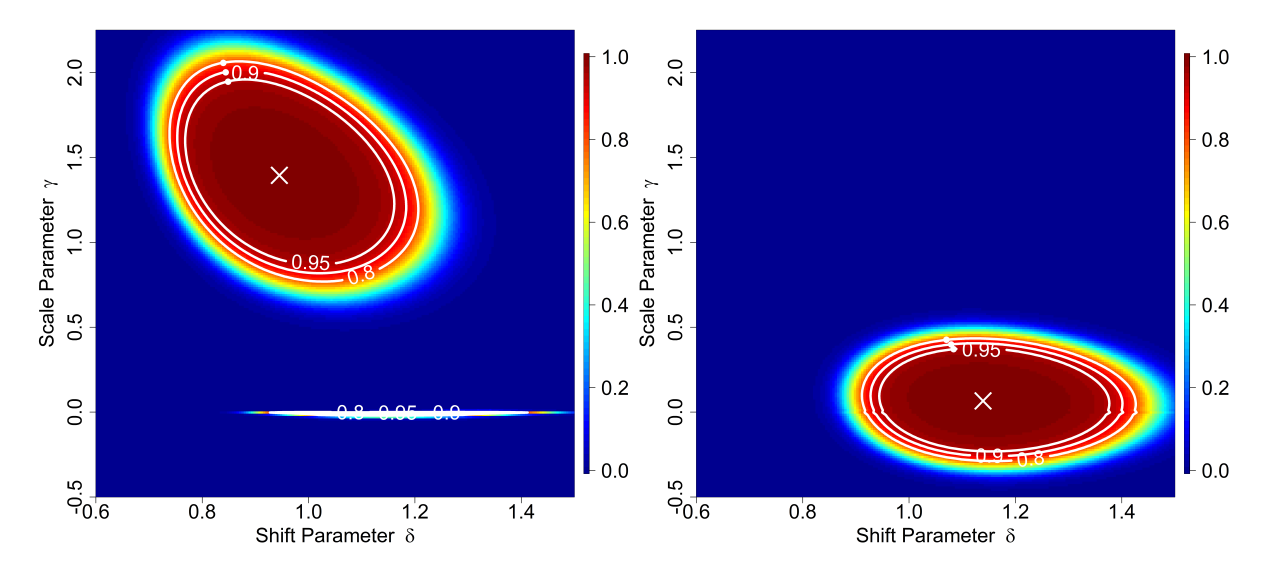


Figure 6: Boldness-recalibration contour plots for FiveThirtyEight (Left) and Random Noise (Right). Regions in red reflect high $P(M_c|\mathbf{y})$ for the LLO-adjusted \mathbf{x} via corresponding δ (x-axis) and γ (y-axis) values. Regions in blue show low $P(M_c|\mathbf{y})$. The × marks $\hat{\delta}_{MLE}$ and $\hat{\gamma}_{MLE}$ where the probability of calibration is maximized. Contours at t = 0.95, 0.9, and 0.8 are drawn in white and $\hat{\delta}_t$ and $\hat{\gamma}_t$ are marked by white points along each contour.

Five Thirty Eight (Left) and the Random forecaster (Right) change under LLO-adjustments via MLEs and boldness recalibration. The first column of points in each panel represents the original set of probability predictions. The second column of points represents the predictions after recalibrating with the MLEs. The third, fourth, and fifth columns of points represent the predictions after 95%, 90%, and 80% boldness-recalibration respectively. A line is used to connect each original prediction to where it ends up after each recalibration procedure. Points and lines colored blue correspond to predictions for games in which the home team won. Red corresponds to games in which the home team lost. The posterior model probability of calibration is reported in the parentheses in the axis label. Note that the posterior model probabilities are not necessarily linear from left to right. We order the sets in this way, starting with the original forecasters sets, to make consistent comparisons throughout the results of the paper.

First, notice that by maximizing $P(M_c|\mathbf{y})$, the range of FiveThirtyEight's predictions expands from (0.26, 0.77) to (0.18, 0.84), whereas the spread of Random Noise contracts from (0.26, 0.77) to (0.51, 0.55). FiveThirtyEight can achieve a maximal probability of

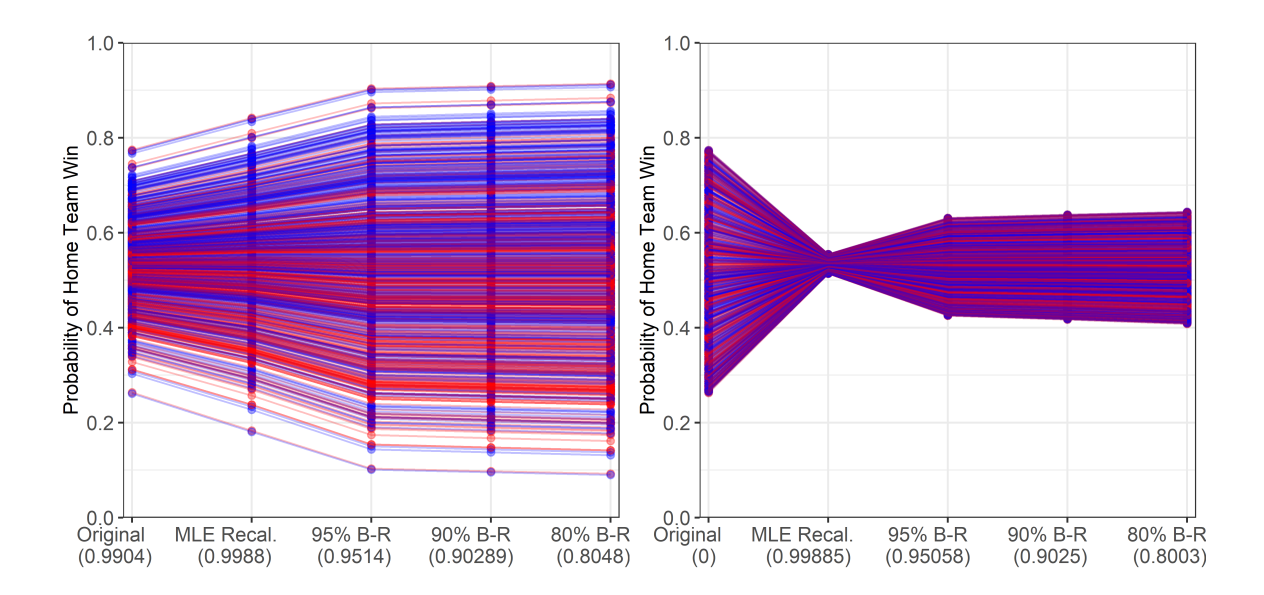


Figure 7: Lineplot visualizing how the predictions for FiveThirtyEight (Left) and the Random forecaster (Right) change under LLO-adjustments via MLEs and boldness recalibration. The first column of points in each panel is the original set of probability predictions. The second column of points is the predictions after recalibrating with the MLEs. The last three columns are the predictions after 95%, 90%, and 80% boldness-recalibration respectively. A line is used to connect each original prediction to where it ends up after each recalibration procedure. Points and lines colored blue correspond to predictions for games in which the home team won. Red corresponds to games in which the home team lost. Achieved $P(M_c|\mathbf{y})$ is reported in the parentheses in the axis label.

calibration of 0.9988, as seen in Table 3. In contrast, for Random Noise to achieve their maximal calibration of 0.9989, they must pull their predictions in toward the base rate of 0.53. Not only does this imply the Random forecaster is poorly calibrated, but it also suggests that their predictions do not have useful predictive information. We know this to be true because these predictions were randomly generated with no association with the outcome.

Next, compare the spread of original predictions to the spread of the 95% boldness-recalibration set. FiveThirtyEight can further embolden their predictions by accepting a 5% risk of mis-calibration, expanding their range to (0.10, 0.90). This suggests that FiveThirtyEight could embolden predictions with a modest decrease in $P(M_c|\mathbf{y})$, where

	FiveThirtyEight				Random Noise					
	$\hat{\delta}$	$\hat{\gamma}$	$P(M_c \mathbf{y})$	Prediction Range		$\hat{\delta}$	$\hat{\gamma}$	$P(M_c \mathbf{y})$	Prediction Range	
MLE	0.945	1.401	0.9988	0.181	0.842	1.140	0.072	0.9989	0.514	0.555
95% B-R	0.849	1.946	0.9514	0.101	0.904	1.098	0.315	0.9506	0.425	0.631
90% B-R	0.844	2.001	0.9029	0.095	0.909	1.057	0.329	0.9025	0.417	0.638
80% B-R	0.840	2.057	0.8048	0.090	0.914	1.061	0.357	0.8003	0.408	0.644

Table 3: Values of the posterior model probability of calibration $P(M_c|\mathbf{y})$ and range achieved under MLE recalibration, 95%, 90%, and 80% boldness-recalibration (B-R) via estimated adjustment parameters $\hat{\delta}$ and $\hat{\gamma}$ for FiveThirtyEight and Random Noise.

the Random Noise forecaster has no knowledge of the outcome and should make far more cautious calls. Boldness-recalibration successfully increases the boldness of our skilled hockey forecaster while maintaining an user-specified level of calibration, putting them in the center of the Venn Diagram in Figure 1 as desired.

3.2.3 Foreclosure Monitoring Case Study

Figure 8 shows that the out of sample predicted probabilities of foreclosure from Keefe et al. (2017) are poorly calibrated and 95% boldness-recalibration has a large effect on boldness corrects bias. Despite this miscalibration, Classification accuracy is high and thus the predictions are emboldened under boldness-recalibration. The posterior model probability of calibration achieved by the original predictions is 0.000. Relaxing calibration to \sim 0.95 expands the range from (0.06, 0.60) to (0.20, 0.96) and shifts the average prediction from 0.3815 to the base rate of 0.7974.

3.2.4 Medical Imaging Case Study

Figure 9 shows that the predicted probabilities that a chest CT will be ordered (Levine et al. 2013) are highly calibrated and 95% boldness-recalibration has a large effect on boldness. The posterior model probability of calibration achieved by the original predictions is 0.9999. Relaxing calibration to ~ 0.95 expands the range of predictions from (0.00, 0.47) to (0.00, 0.47)

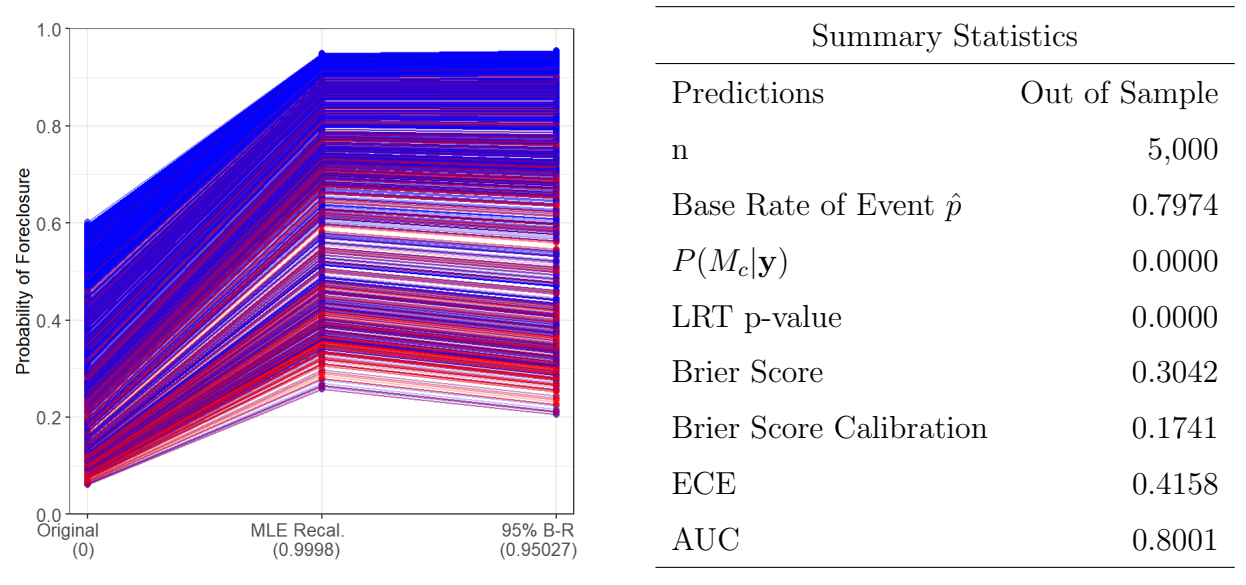


Figure 8: Lineplot showing that predicted probabilities of foreclosure are poorly calibrated $(P(M_c|\mathbf{y}) = 0)$ and 95% boldness-recalibration highly increases boldness and corrects bias.

0.54). This is the maximal amount of boldness achievable at this level of calibration and classification accuracy.

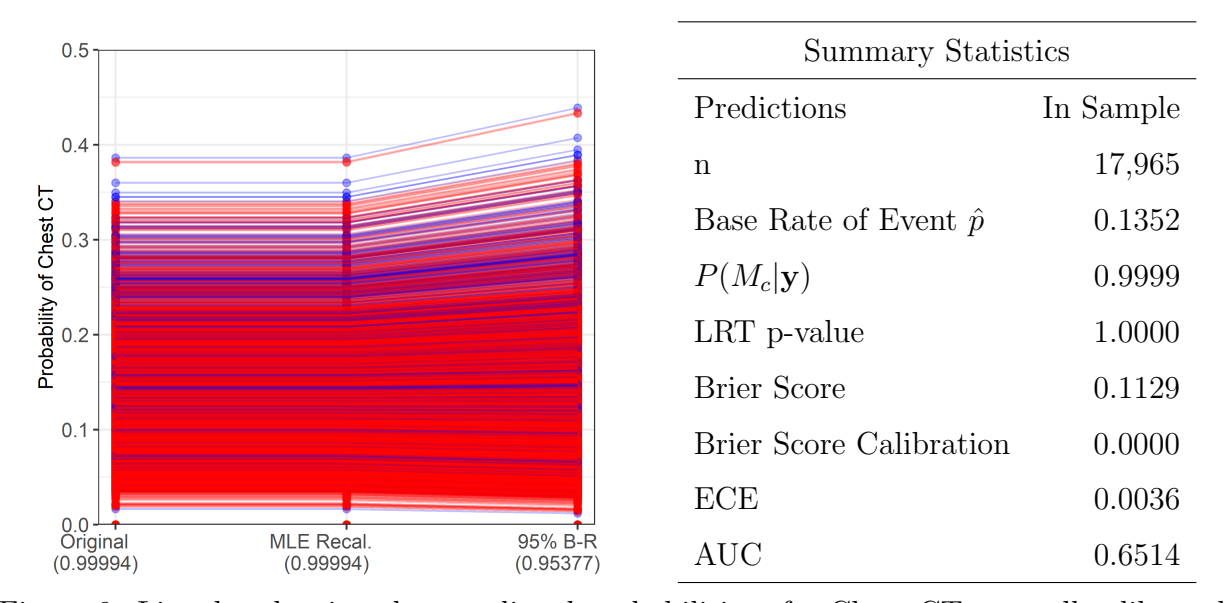


Figure 9: Lineplot showing that predicted probabilities of a Chest CT are well calibrated $(P(M_c|\mathbf{y}) = 0.9999)$ and 95% boldness-recalibration increases boldness. Note that due to the large sample size, only 20% of the data randomly selected is plotted.

3.2.5 Oscars Case Study

Figure 10 shows that the predicted probabilities that a movie will win the Academy Award for best picture (Franck & Wilson 2021) are highly calibrated and 95% boldness-recalibration has a small effect on boldness. The posterior model probability of calibration achieved by the original predictions is 0.9972. Relaxing calibration to \sim 0.95 expands the range of predictions from (0.00, 0.96) to (0.00, 0.98).

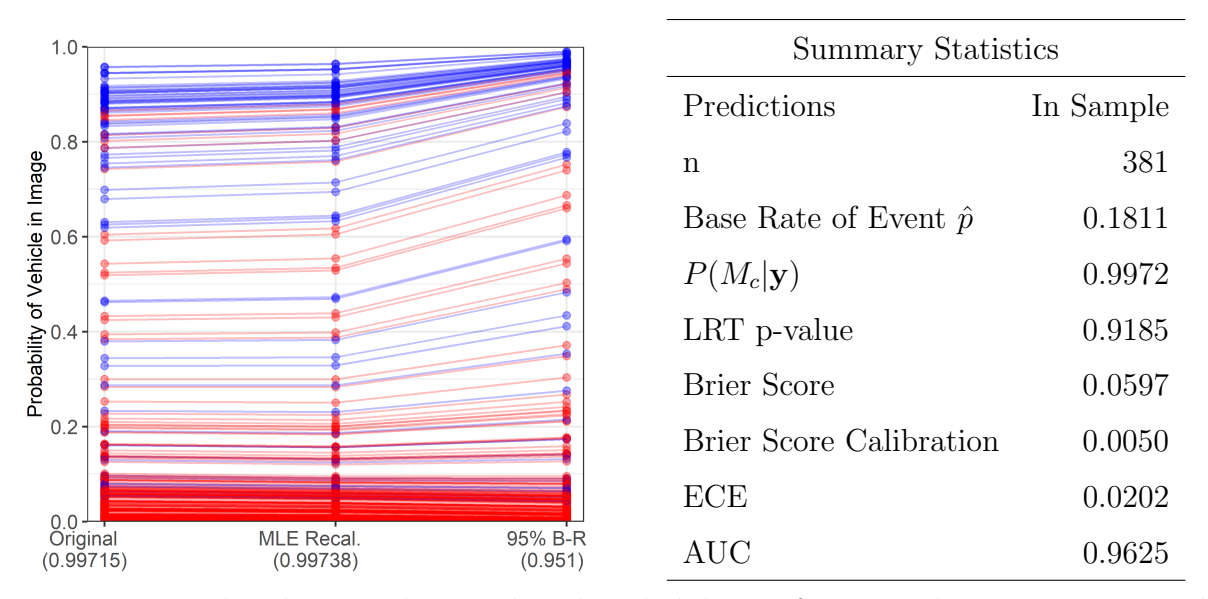
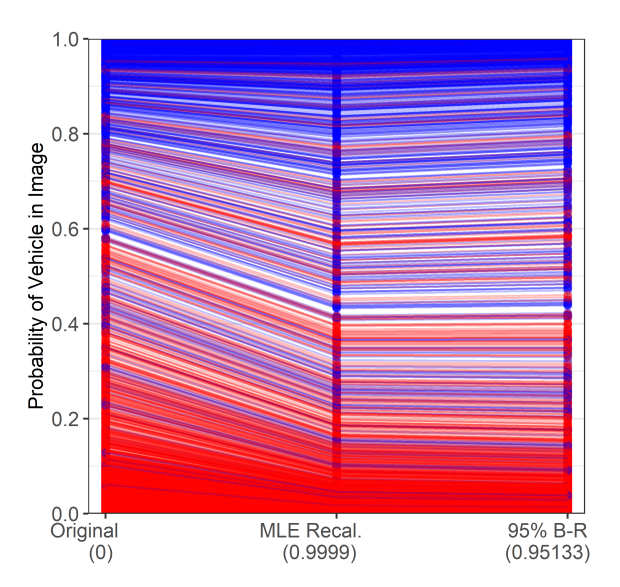


Figure 10: Lineplot showing that predicted probabilities of winning best picture are well calibrated $(P(M_c|\mathbf{y}) = 0.9972)$ and 95% boldness-recalibration increases boldness.

3.2.6 Neural Net Image Classification Case Study

Figure 11 shows that the out of sample probability predictions for when an image contains a vehicle are not well calibrated and 95% boldness-recalibration has a large effect on the predictions and corrects bias. The probability these predictions are well calibrated is 0.000. Via 95% boldness-recalibration, the range expands from (0.06, 0.60) to (0.20, 0.96) and shifts the average prediction from 0.4556 to the base rate of 0.4000.



Summary Statistics					
Predictions	Out of Sample				
n	10,000				
Base Rate of Event \hat{p}	0.4000				
$P(M_c \mathbf{y})$	0.0000				
LRT p-value	0.0000				
Brier Score	0.0730				
Brier Score Calibration	0.0057				
ECE	0.0556				
AUC	0.9685				

Figure 11: Lineplot showing that predicted probabilities of vehicles in the CIFAR-10 image data set are poorly calibrated $(P(M_c|\mathbf{y}) = 0)$ and 95% boldness-recalibration increases boldness and corrects bias. Note that due to the large sample size, only 20% of the data randomly selected is plotted.

4 Conclusion

This paper develops boldness-recalibration methodology surrounding the fundamental tension between calibration and boldness of predicted probabilities, subject to classification accuracy. Few methods consider boldness relative to calibration; even fewer, if any, provide a clear interpretation of the trade-off between these key aspects. Our proposed Bayesian calibration assessment and boldness-recalibration approaches address this gap.

The backbone of these approaches is the interpretable posterior model probability, $P(M_c|\mathbf{y})$, which serves as a measure of calibration and is interpreted as the probability a set of predictions is calibrated, given the data observed. In boldness-recalibration, the user pre-specifies a tolerable risk of miscalibration (e.g. $P(M_c|\mathbf{y}) = 0.95$) and subject to this constraint, our method maximizes spread in predictions and thus, boldness. The difference in the posterior model probabilities for the original and boldness-recalibrated sets concisely quantifies the calibration-boldness trade-off.

We verify via simulation study that our calibration assessment approaches correctly identify miscalibration in nearly all forecaster types at a reasonable sample size. Our

approaches also suggest that a real-world Hockey forecaster, FiveThirtyEight, is well calibrated and correctly identifies the Random Noise forecaster as poorly calibrated. In our array of four other case studies, we examine predictions from the fields of economics, medicine, entertainment, and machine learning image recognition. Two of the four prediction sets are deemed well calibrated by our approach.

While $P(M_c|\mathbf{y})$ and the LRT p-values for calibration generally agree with the Brier Score, BSC, and ECE, we argue that $P(M_c|\mathbf{y})$ is more readily interpretable than these metrics. While FiveThirtyEight achieves a lower Brier Score of 0.23 compared to Random Noise with a score of 0.27, it is difficult to determine how much better FiveThirtyEight is or if either score is actually considered "good". Prospectively determining a "good" Brier Score or ECE for a specific application is challenging where specifying a desired probability of calibration is clear.

We also show how $P(M_c|\mathbf{y})$ can be used to set the specified level of calibration and interpret the trade off between calibration and boldness in our five case studies via boldness-recalibration. This approach successfully emboldens FiveThirtyEight while maintaining the user-specified levels of calibration. However, boldness-recalibration showed that the Random Noise forecaster should bring their predictions in towards the base rate rather than embolden. In all of the other four case studies, classification accuracy is relatively high and thus predictions are emboldened under 95% boldness-recalibration. This is true even when miscalibration is present in the original predictions as the miscalibration is corrected.

While we provide a limited set of use-cases in this paper, we propose these methods are useful in many situations where there are predicted probabilities of binary event. These methods allow decision makers to rely on these predictions for make informed decisions. Appropriately emboldened predictions, as produced by Boldness-recalibration in an interpretable manner, enable better decision making in these critical situations.

Acknowledgements

The authors would like to thank Chris Wilson, Damon Kuehl, Matthew Keefe, Andrew McCoy, and Bill Woodall for their roles obtaining case study data for this project. The

authors would like to thank Metrostudy, a HanleyWood Company for providing the data used in the foreclosure case study. The authors would like to thank Tyler Cody and Xin Xing for helpful background information about probability calibration and neural networks.

References

Atanasov, P., Rescober, P., Stone, E., Swift, S. A., Servan-Schreiber, E., Tetlock, P., Ungar, L. & Mellers, B. (2017), 'Distilling the wisdom of crowds: Prediction markets vs. prediction polls', *Management Science* **63**(3), 691–706.

URL: https://doi.org/10.1287/mnsc.2015.2374

- Baron, J., Mellers, B. A., Tetlock, P. E., Stone, E. & Ungar, L. H. (2014), 'Two reasons to make aggregated probability forecasts more extreme', *Decision Analysis* 11(2), 133–145. URL: https://doi.org/10.1287/deca.2014.0293
- Brier, G. W. (1950), 'Verification of forecasts expressed in terms of probability', Monthly Weather Review 78(1), 1-3.
- Bross, I. D. J. (1953), Design for Decision, New York: Macmillan.
- Dalton, J. E. (2013), 'Flexible recalibration of binary clinical prediction models', *Statistics in Medicine* **32**(2), 282–289.
- Dawid, A. P. (1982), 'The well-calibrated bayesian', Journal of the American Statistical Association 77(379), 605–610.
- DeGroot, M. H. & Fienberg, S. E. (1983), 'The comparison and evaluation of forecasters', Journal of the Royal Statistical Society. Series D (The Statistician) 32(1/2), 12–22.
- Franck, C. T. & Wilson, C. E. (2021), 'Predicting competitions by combining conditional logistic regression and subjective Bayes: An Academy Awards case study', *The Annals of Applied Statistics* **15**(4), 2083 2100.

URL: https://doi.org/10.1214/21-AOAS1464

- Gonzalez, R. & Wu, G. (1999), 'On the shape of probability weighting function', *Cognitive Psychology* **38**, 129–66.
- Guo, C., Pleiss, G., Sun, Y. & Weinberger, K. Q. (2017), 'On calibration of modern neural networks', *CoRR* abs/1706.04599.

URL: http://arxiv.org/abs/1706.04599

- Han, Y. & Budescu, D. V. (2022), 'Recalibrating probabilistic forecasts to improve their accuracy', *Judgement and Decision Making* 17, 91–123.
- Kass, R. E. & Raftery, A. E. (1995), 'Bayes factors', Journal of the American Statistical Association 90(430), 773–795.
- Keefe, M. J., Franck, C. T. & Woodall, W. H. (2017), 'Monitoring foreclosure rates with a spatially risk-adjusted bernoulli cusum chart for concurrent observations', *Journal of Applied Statistics* **44**(2), 325–341.

URL: https://doi.org/10.1080/02664763.2016.1169257

- Krizhevsky, A., Hinton, G. et al. (2009), 'Learning multiple layers of features from tiny images'.
- Levine, M. B., Moore, A. B., Franck, C., Li, J. & Kuehl, D. R. (2013), 'Variation in use of all types of computed tomography by emergency physicians', *The American Journal of Emergency Medicine* **31**(10), 1437–1442.

URL: https://www.sciencedirect.com/science/article/pii/S0735675713004452

- Lichtendahl, K. C., Grushka-Cockayne, Y., Jose, V. R. R. & Winkler, R. L. (2022), 'Extremizing and anti-extremizing in bayesian ensembles of binary-event forecasts', *Operations Research*.
- Murphy, A. H. (1972), 'Scalar and vector partitions of the probability score: Part i. two-state situation', *Journal of Applied Meteorology* 11, 1183–1192.
- Murphy, A. H. (1973), 'A New Vector Partition of the Probability Score.', *Journal of Applied Meteorology* **12**(4), 595–600.

- Murphy, A. H. & Winkler, R. L. (1977), 'Reliability of subjective probability forecasts of precipitation and temperature', *Journal of the Royal Statistical Society. Series C (Applied Statistics)* **26**(1), 41–47.
- Naeini, M. P., Cooper, G. & Hauskrecht, M. (2015), 'Obtaining well calibrated probabilities using bayesian binning', *Proceedings of the AAAI Conference on Artificial Intelligence* **29**(1).
- Platt, J. (2000), 'Probabilistic outputs for support vector machines and comparisons to regularized likelihood methods', Adv. Large Margin Classif. 10.
- Roitberg, A., Peng, K., Schneider, D., Yang, K., Koulakis, M., Martínez, M. & Stiefelhagen, R. (2022), 'Is my driver observation model overconfident? input-guided calibration networks for reliable and interpretable confidence estimates', *ArXiv* abs/2204.04674.
- Turner, B., Steyvers, M., Merkle, E., Budescu, D. & Wallsten, T. (2014), 'Forecast aggregation via recalibration', *Machine Learning* **95**, 261–289.
- Zadrozny, B. & Elkan, C. P. (2001), Obtaining calibrated probability estimates from decision trees and naive bayesian classifiers, in 'ICML'.
- Zadrozny, B. & Elkan, C. P. (2002), 'Transforming classifier scores into accurate multiclass probability estimates', *Proceedings of the eighth ACM SIGKDD international conference on Knowledge discovery and data mining*.

Supplemental material for $Calibration \ Assessment \ and$ $Boldness-Recalibration \ for \ Binary \ Events$

4.1 Case Studies

4.1.1 Hockey Home Team Win Predictions

FiveThirtyEight provided their predictions in the form of a downloadable spreadsheet with the predicted probabilities of a home team win or away team win on their website (https://

data.fivethirtyeight.com/). The win/loss game results were obtained by web-scraping from NHL.com using the NHL API. These results were then mapped to the probabilities forecasts of FiveThirtyEight by matching by game date and teams. FiveThirtyEight's predictions are compiled from year to year, so the data for the 2020-21 season is included in the same downloadable spreadsheet as the most recent season's predictions. This data set was used because it is publicly available online, it provided a complete seasons worth of game observations, and it display properties that we were particularly interested in exploring via our method.

An important thing to note about the 2020-21 NHL season that distinguishes it from other seasons is that it comes on the heels of an abbreviated 2019-20 season due to the COVID-19 pandemic. With the previous season significantly shortened and playoff pushed to the end of summer, the 2020-21 season started late in comparison to a "normal" NHL season and consisted of only 56 games per team instead of the "normal" 82 games per team. Additionally, teams were restricted to only playing within their division, with divisions realigned to minimize travel. While these abnormalities do not directly affect the validity of our methodology, they should be kept in mind when comparing forecaster predictions from this season to other seasons.

4.1.2 Foreclosure Monitoring Predictions

The foreclosure monitoring case study arises from a project that developed a monitoring strategy for the housing market using a spatially-adjusted model of foreclosure risk (Keefe et al. 2017). The probability of foreclosure was estimated using a mixture model of spatial kernel density estimates, with one component of the mixture corresponding to healthy sales and the other component corresponding to foreclosures. The model was trained during the first six months of 2005 using data from Wayne County, Michigan in the first six months of 2005, which is a pre-Great Recession time period. The original study used this spatial risk adjustment within a CUSUM chart to monitor the housing market from the second half of 2005 thru 2014.

For this case study, we illustrate our calibration assessment and boldness-recalibration using 5,000 randomly selected housing transactions in 2010. We anticipated (correctly)

that foreclosure forecasts using our model trained on data from before the Great Recession would be badly calibrated in the midst of the Great Recession (mostly due to wildly underestimating foreclosure rates).

4.1.3 Medical Ordering Predictions

The medical ordering case study comes from (Levine et al. 2013), which examined variability in ordering rates of imaging among emergency room physicians. Imaging is a powerful but costly medical diagnostic technique, so quantification of ordering variability is important to study in the context of healthcare. The original paper modeled ordering rates as a function of physician ID, emergency severity index, patient age, time of day of visit, and the patient's disposition (discharged, admitted, deceased, etc.).

The probability forecasts in this paper are based on the 17,965 records from this project using the above model and de-identified data. Patients chief complaint was chest pain and the outcome variable being modeled was a binary (Yes/No) ordering division for chest imaging from each physician.

4.1.4 Academy Award Predictions

The Academy Award case study predicts which film will win the top award for best picture (Franck & Wilson 2021). The original project used data from 1950-2018 to predict win probabilities for movies in the year 2019. The original modeling framework used conditional logistic regression and approximate Bayesian model averaging, and allowed a broad readership of Time.com to interactively fuse their own predictions with the model's predictions (see https://time.com/5779417/oscars-best-picture-prediction/).

For this project, the probability predictions we used are the 381 model averaged predictions from years 1950-2018.

4.1.5 Image classification predictions

Within the context of machine learning and pattern recognition, we consider predicted probabilities from a rudimentary convolutional neural network for image classification using the CIFAR-10 training data set (Krizhevsky et al. 2009). The CIFAR-10 data set includes

ten classifications of images, which are 'plane', 'car', 'bird', 'cat', 'deer', 'dog', 'frog', 'horse', 'ship', and 'truck'. We group these labels into two categories: 'vehicle' and 'animal'. The probability forecasts for these categories are based on the 10,000 images in the CIFAR test set. We lightly edited the code at the following link to obtain predictions.

https://pytorch.org/tutorials/beginner/blitz/cifar10_tutorial.html

4.2 Boldness recalibration

Below are steps to formalize the Boldness-Recalibration procedure:

- 1. Set the minimum calibration level, t, e.g. t = 0.95.
- 2. Let $\Delta = (\delta_1, ..., \delta_k)$ and $\Gamma = (\gamma_1, ..., \gamma_k)$ form a set of potential values for δ and γ .
- 3. LLO-adjust **x** under each δ_i , γ_j pair to produce transformed probabilities $x'_{ij} = c(x; \delta_i, \gamma_j)$, i = 1, ..., k and j = 1, ..., k.
- 4. To measure calibration, calculate $P(M_1|\mathbf{y}, \delta_i, \gamma_j)$ for each x'_{ij} .
- 5. To quantify spread (i.e. boldness) in transformed probabilities, let s_{ij} be the standard deviation of x'_{ij} .
- 6. The recalibrated set which maximizes spread given calibration

$$x_{B-R}^t = argmax_{x'_{ij}}(s_{ij} : P(M_1|\mathbf{y}, \delta_i, \gamma_j) \ge t)$$

is called the (100 * t)% Boldness-Recalibration set. We denote the parameters that generate x_{B-R}^t as $\hat{\delta}_t$ and $\hat{\gamma}_t$.

Throughout the case studies presented, we used k=200 to form a grid of potential δ and γ values in step 2. The ranges for δ and γ vary depending on the data set. While forming a grid is not the only way to select δ and γ values, we provide some guidance below for grid selection.

Some care is required for the selection of the range of δ and γ values you examine and the size of k, which together determine the fineness of your grid of parameter values.

First, it is important to determine what values of δ and γ to consider for effective boldness-recalibration. By "potential" in step (2), we mean the range of parameter values which encompasses the region of non-zero posterior probabilities of calibration. Since neither of these parameters are fully bounded, we cannot form a grid over the entire parameter space for the regions which produce well calibrated probabilities. Instead, we could look at a finite, but still very large, set of parameter values which encompass all plausible settings. Under this approach, we may search over $\delta \in (0, 100)$ and $\gamma \in (-75, 75)$. However, unless k is extremely large which creates a very fine grid, you may not be able to detect the region in which non-zero posterior probabilities are produced, as the region is often quite small relative to the entire parameter space. This is problematic, as computation time increases as k grows.

We suggest the following scheme for determining the grid of parameter values to search. First, fix k at some small number, less than 20 for sake of computation time. Then, center a grid with small range around $\hat{\delta}_{MLE}$ and $\hat{\gamma}_{MLE}$ for x. Increase the size of k until your grid detects approximated the probability of calibration at the MLEs that you expect. At this point, you may find that your grid does not fully encompass the range of parameters values which produce recalibrated probabilities with meaningfully high posterior probability of being calibrated. If this is the case, expand your grid until it the region with high probability of calibration is covered. Then, increase k to create a fine grid of values.

4.3 Connection to Logistic Regression

Our approach of adopting a Bernoulli Likelihood governed by LLO-adjusted probabilities is equivalent to a specialized logistic regression model. As established, our outcome $y \sim \text{Bernoulli}(p)$. We have a linear predictor in the form of $\eta = X\beta = \gamma log\left(\frac{x}{1-x}\right) + \tau$. Lastly, we have the logit link such that $\eta = log\left(\frac{p}{1-p}\right)$ The key difference between standard logistic regression and our approach is that we let p = c(x), or in words, we let the governing probabilities of our outcomes equal the LLO-adjusted probabilities from the LLO function.

4.4 Additional Simulation Study Results

Figures 12, and 13 summarize the overall Brier Score and Expected Calibration Error (ECE) for the 100 MC runs. On each figure, the boxplots are grouped by simulated forecaster type shown on the x-axis. The y-axis shows the value of the metric of interest. Sample size increases with vertical panels from top to bottom. Within each group of boxplots, added noise σ increases from left to right. Thus, for the Well Calibrated group, only the first boxplot with no added noise ($\sigma = 0$) is perfectly calibrated and calibration decreases as added noise increases.

Figure 12 shows that as sample size increases the variability in the Brier Score decreases but the average remains approximately the same for all settings. Recall that lower Brier Score are better, however, the Brier Score is not a direct measure of calibration. Unlike posterior probability of calibration, it is difficult to interpret an individual forecaster's Brier Score in isolation, especially in terms of calibration.

Figure 13 shows that as sample size increases the ECE decreases for all settings, not just those that are well calibrated. Recall smaller ECE is better. While ECE provides greater distinction between forecasters than the Brier Score Calibration Component (BSC) it is still difficult to interpret an individual forecaster's ECE in isolation.

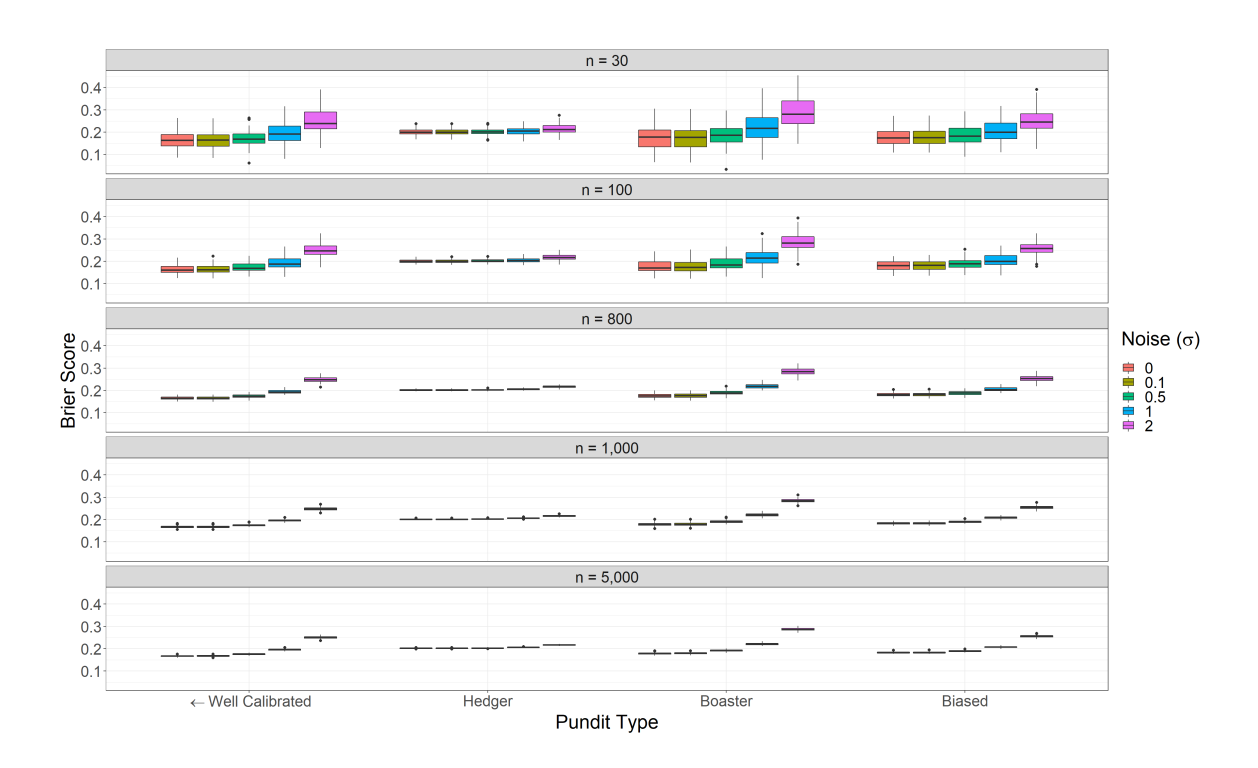


Figure 12: Boxplots summarizing the Brier Score on the y-axis for 100 MC runs on simulated forecasters. Boxplots are grouped by forecaster type on the x-axis. Within groups, added noise increases from left to right. Only the leftmost boxplot in the Well Calibrated group is perfectly calibrated, and \leftarrow indicates calibration increases as noise decreases.

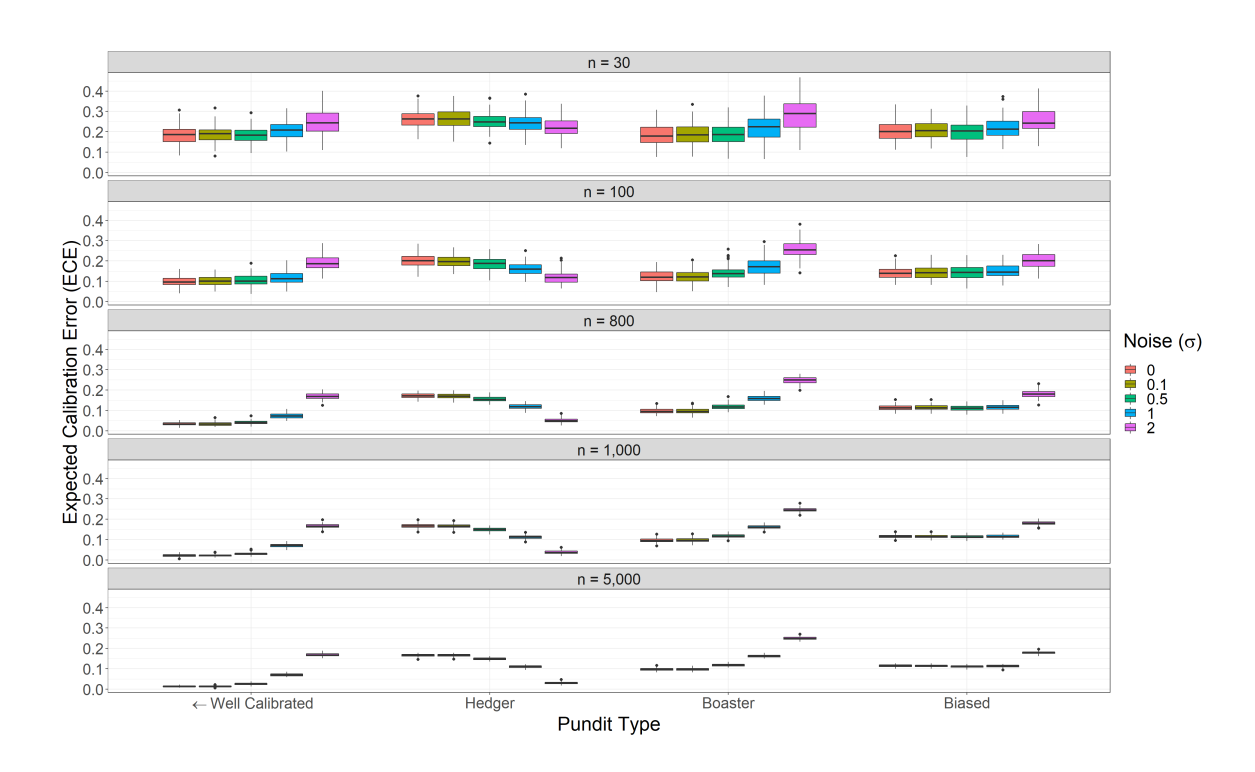


Figure 13: Boxplots summarizing the ECE on the y-axis for 100 MC runs on simulated forecasters. Boxplots are grouped by forecaster type on the x-axis. Within groups, added noise increases from left to right. Only the leftmost boxplot in the Well Calibrated group is perfectly calibrated, and \leftarrow indicates calibration increases as noise decreases.